NUCL SCI TECH (2016) 27:9
DOI 10.1007/s41365-016-0008-7

Zeolitic imidazolate framework-8 as a nanoadsorbent for radon capture

Xiao-Wa Wang[1,2,3,4] · **Ting Yan**[5] · **Jun Wan**[1,2,3,4] ·
Li-Feng Zhao[5] · **Yu Tu**[1,2,3,4]

Received: 20 March 2015 / Revised: 1 June 2015 / Accepted: 2 June 2015 / Published online: 27 February 2016

Abstract The feasibility of adsorption and the adsorption behavior of radon on a nanomaterial-based zeolitic imidazolate framework-8 (ZIF-8) adsorbent were investigated. Grand canonical Monte Carlo simulation and four-channel low-background α/β measurement were performed to examine the adsorption kinetics of this adsorbent. Results demonstrated that ZIF-8 is a good adsorbent of radon. Therefore, this adsorbent can be used to significantly reduce the hazardous effects of radon on occupational radiation workers.

Keywords Zeolitic imidazolate framework-8 · Radon · Adsorption

1 Introduction

Nuclear fuel reprocessing or inadvertent environmental release yields volatile gaseous fission products; however, capturing these products remains a challenge [1]. Common gaseous radionuclides include ^{129}I, ^{131}I, ^{3}H, $^{14}CO_2$, ^{85}Kr and ^{86}Rn. Among these radionuclides, radiological Rn has been extensively investigated because this substance can be used in many applications. Rn has radioactive isotopes under normal conditions. Rn is also considered as a health hazard because it exhibits radioactivity. Rn is a noble, colorless, and tasteless gas. As such, this gas cannot be easily detected by the senses. As a highly mobile gas, Rn poses risks to organisms exposed to Rn isotopes. Among the Rn isotopes, ^{222}Rn is the most stable, with a half-life of 3.8 days. Despite this stable nature, ^{222}Rn cannot be captured and reliably stored before this isotope decays. Other isotopes are short-lived (half-life of an hour or second); these isotopes should also be immediately captured because these substances directly affect human metabolic processes. In the USA, Rn can accumulate in the lungs of non-smokers, thereby causing lung cancer [2].

Clean, safe and responsible adsorption materials should be developed to satisfy increased demands for worldwide healthy environments and to reduce radioactive gas emissions, such as underground construction [3]. Therefore, separation methods have been established via selective adsorption at non-cryogenic temperatures on microporous materials, such as zeolites and activated carbon [4]. These materials are robust, but lack high adsorption capacities because of limited surface areas.

Compared to zeolites, metal-organic frameworks (MOFs) represent a new class of functional materials containing metal centers linked to organic building blocks to produce diverse and customizable structural frameworks [5]. These materials have been extensively investigated because of several properties, such as high structural stability, large surface areas, large and structurally flexible

---

✉ Yu Tu
tuyu@suda.edu.cn

[1] School of Radiation Medicine and Protection, Medicine College of Soochow University, Suzhou 215123, China

[2] School for Radiological and Interdisciplinary Sciences, Suzhou 215123, China

[3] Collaborative Innovation Center of Radiation Medicine of Jiangsu Higher Education Institutions, Suzhou 215123, China

[4] Jiangsu Provincial Key Laboratory of Radiation Medicine and Protection, Suzhou 215123, China

[5] National Institute of Biological Sciences, Beijing 102206, China

pore structures, and adjustable chemical functionalities. The pore size and the shape of these porous materials play a decisive role. The structure of MOFs can also be modified to enhance sorbate–sorbent interactions [6]. MOFs have been applied as an adsorbent of noble gases [7–10]. As a subfamily of MOFs, zeolitic imidazolate frameworks (ZIFs) exhibit highly desirable properties of zeolites and MOFs, such as permanent porosity, uniform pore size, and exceptional thermal and chemical stability [11]. With these excellent characteristics, ZIFs are potential candidates to increase Rn adsorption. Noble gases have also been extensively explored, particularly storage and separation of noble gases using MOFs [12–17]. Nevertheless, whether MOFs can adsorb Rn or not remains unknown.

In this study, the efficacy of ZIF-8 as a high-capacity Rn adsorbent was investigated for the first time. ZIF-8 was carefully selected from a broad library of potential MOFs and used as an efficient trap to capture molecular Rn because this substance is characterized by the suitable pore aperture size, large specific surface area, and high chemical and thermal stability. Tetrahedrally coordinated Zn atoms linked by 2-methylimidazole (MeIM) ligands constitute ZIF-8 with a network of an expanded sodalite structure. β-cages, with a diameter of 11.6 Å, are connected via six-membered-ring (6MR) apertures with a diameter of 3.4 Å in the directional diffusion of Rn (3.35 Å) instead of smaller four-membered-ring (4MR) windows, which are constrained, preventing the diffusion of guest molecules. A ZIF-8 framework and its associated pore network are highly symmetric, posing particular challenges in locating guest molecules, which are often crystallographically disordered. Thus, guest binding can be fully understood by summarizing information related to not only the local and long-range structural probes, but also the molecular simulations. ZIF-8 is synthesized using several efficient methods [18–22], such as rapid room-temperature synthesis [23]. High-resolution synchrotron-based powder X-ray diffraction (PXRD), grand canonical Monte Carlo (GCMC) analysis, and molecular dynamics simulations are also applied to identify the quasi-perfect binding sites of molecular Rn in ZIF-8. The structure–property relationship between an occluded gas molecule and a host framework was also investigated in this study.

2 Materials and method

2.1 Materials

Zinc nitrate hexahydrate ($Zn(No_3)_2{\cdot}6H_2O$; AR, Sinopharm Chemical Reagent Co., Ltd.), 2-Methylimidazole (MeIM) (99 %, Sinopharm Chemical Reagent Co., Ltd.), and anhydrous methanol (AR, Sinopharm Chemical Reagent Co., Ltd.) were used as received.

2.2 Synthesis and characterization of ZIF-8

ZIF-8 was synthesized in accordance with a previously described method [23]. In brief, a solution of $Zn(No_3)_2{\cdot}6H_2O$ and Meim was prepared using anhydrous methanol as a solvent with a molar ratio of approximately 1:8:700. X-ray diffraction (XRD) patterns were recorded using a powder X-ray diffractometer/X'Pert-Pro MPD (Philips). Thermal gravimetric analysis (TGA) was performed on a PTC-10A thermal gravimetric analyzer (TA, America) from room temperature to 600 °C at a ramp rate of 10 °C/min under a nitrogen flow of 20 mL/min. Nitrogen sorption experiments were performed at 77 K on a Micromeritics ASAP 2010 sorption analyzer after a sample (ca. 0.05 g) was activated at 120 °C for 12 h in a primary vacuum.

2.3 GCMC simulations of ZIF-8 adsorption of Rn

GCMC simulations of Kr and Rn on ZIF-8 were conducted separately to validate experimental results and understand the adsorption molecular details.

The universal force field [24] parameters of ZIF-8 were used in GCMC simulations in accordance with previously described procedures [25]. Force field parameters of Kr and Rn were optimized in accordance with the parameterization procedure of Sun [26]. In this procedure, molecular dynamics simulations were applied to reproduce the experimental data of liquid density and heat of vaporization at 117 and 210 K, respectively. The structure of ZIF-8 was established in accordance with the method proposed by Moggach et al. [27]. GCMC simulations were conducted at 308 K from 0.01 bar to 20 bar. Atomic moves, such as insertion, deletion, and translation of Kr or Rn, were also induced in the simulations. The positions of ZIF-8 atoms were tightly fixed. In each simulation, 1,000,000 moves were facilitated to equilibrate the system, followed by 1,000,000 moves to perform a production run. GCMC simulations were prepared using TOWHEE codes [28] (version 7.0.4). Molecular dynamics simulations were prepared using Gromacs codes [29] (version 4.6.5).

2.4 Passive Rn adsorption of ZIF-8

Passive Rn adsorption was conducted by placing 160 mg of ZIF-8 in a chamber containing 100 000 Bq standard Rn for 0, 6, 12, 18, 24, 30 and 36 h. After passive adsorption was completed, each sample was removed and immediately placed in the detector of a four-channel low-background alpha and beta measuring instrument (BH1227, China).

2.5 Active radon adsorption of ZIF-8

Active radon adsorption was carried out according to the system shown in Fig. 1.

In this study, ZIF-8 adsorbed Rn-222 as a radon resource of a standard radon chamber generated from Ra-226 in the following generation pathways: Ra-226 $\xrightarrow{1600\,\text{year}}$ Rn-222. The physical half-life of Rn-222 is 3.82 days. The half-lives of Rn-220 and Rn-219 are 55.6 and 3.96 s, respectively. During adsorption, a filter paper was used to filter decayed Rn isotopes. Hence, ZIF-8 only adsorbs Rn-222 instead of Rn and its isotopes.

2.5.1 *Alpha and beta ray energy spectrometer measurements (1220 Quantulus, USA) of Rn adsorption by ZIF-8*

^{241}Am with an activity of 10.2 Bq is used as a standard source.

In this study, the volume of Rn rooms is 1 m^3; Rn is produced from a solid radium source. In our experiments, Rn concentration levels are 5000 and 100,000 Bq/m^3. The former Rn chamber is used to perform active and repeat adsorption experiments, and the latter is used to conduct passive adsorption experiments. We can assume that Rn concentration is constant because of the following conditions: first, Rn rooms are larger than a pipe system (approximately 100 mL); second, Rn that flows out of ZIF-8 is recycled in a Rn room; third, Rn concentration is distributed in a confined chamber [30]; and fourth, the distance between an inlet and an outlet is sufficiently long. As radon flows through a sample, decayed Rn isotopes are removed using a filter.

In adsorption, RAD-7 was used to monitor the concentration changes. When this instrument displays a stable Rn concentration, a customized adsorption tube is loaded with 200 mg of ZIF-8. As a result, flow rate decreased to 0.75 L/min. After successive measurements were performed for 29 min, ZIF-8 was immediately crushed for further measurements.

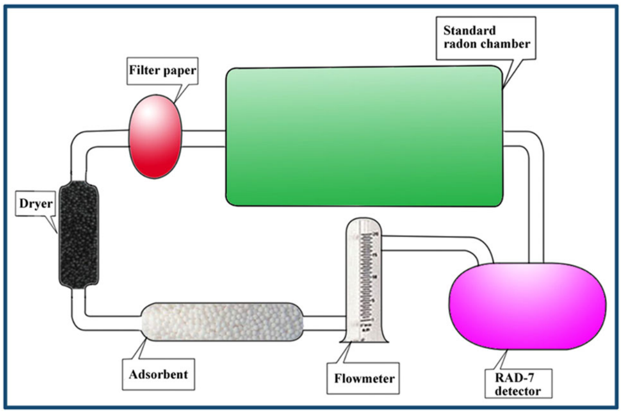

Fig. 1 (Color online) Active adsorption flow chart

2.5.2 *γ-Ray energy spectrometer measurements (GEM40P4-76-RB, USA) of Rn adsorption by ZIF-8*

^{226}Ra with an activity of 524 Bq was used as a standard source.

In adsorption, RAD-7 was used to monitor concentration changes from 0.75 L/min of Rn flow concentration in a monitoring chamber. A customized adsorption tube was loaded with 1 g of ZIF-8 when this instrument displayed a stable Rn concentration. Flow rate was then reduced to 0.55 L/min. After continuous measurement for 70 min, ZIF-8 was immediately crushed for further measurements.

2.6 ZIF-8 reuse for Rn adsorption

After the first Rn adsorption experiment was completed, ZIF-8 was treated in an oven at 100 °C for 24 h. After treatment was administered, the residual Rn in a sample was determined using a four-channel low-background alpha and beta measuring instrument. The results showed that Rn concentration was equal to the natural background level (Table 1). The recycled ZIF-8 was utilized for further Rn adsorption experiments. Adsorption was monitored using an alpha and beta ray energy spectrometer and a γ-ray energy spectrometer.

2.6.1 *Alpha and beta ray energy spectrometer measurement of Rn adsorption by ZIF-8*

Rn concentration in the chamber was monitored from a 0.85 L/min flow. The customized adsorption tube was loaded with 200 mg of ZIF-8 when the instrument displayed a stable radon concentration. The flow rate was then reduced to 0.75 L/min. After continuous measurement was performed for 30 min, ZIF-8 was immediately crushed for further measurements.

2.6.2 *γ-Ray energy spectrometer measurement for Rn adsorption by ZIF-8*

The same conditions were applied. Rn concentration in the chamber was monitored from a 0.85 L/min flow. The customized adsorption tube was loaded with 1 g of ZIF-8 when the instrument displayed stable radon concentration. The flow rate was then reduced to 0.65 L/min. After continuous measurement was performed for 84 min, ZIF-8 was immediately crushed for further measurements.

Table 1 Rn concentration adsorbed on ZIF-8

	Before Rn is adsorbed by α and β ray energy spectrometer		After Rn is adsorbed by α and β ray energy spectrometer	
	α1	β1	α2	β2
Av	7.2	186.5	3.8	170.2
Rb (cps)	0	0.03	0	0.02
A (Bq)	0	0	0.01	0.01

3 Results and discussion

3.1 Synthesis and characterization of ZIF-8

XRD patterns were obtained from a powder sample and compared with a pattern simulated from known structural data [31]; our results demonstrated that the product was a single-phase ZIF-8 material. The nanoscale ZIF-8 powder sample was subjected to TGA; the results revealed that the nanocrystals were stable up to ca. 200 °C in air before the framework structure decomposed. This result indicated that ZIF-8 exhibited the considerable thermal stability. Gas sorption analyses were conducted using the ASAP equipment; the results showed that the nanoscale ZIF-8 powder exhibited permanent microporosity. N_2 sorption isotherms (Fig. 2) also revealed an apparent specific surface area of 1517 m^2/g (BET method) and a micropore volume of 0.58 cm^3/g of the evacuated nanocrystals. These values are slightly lower than the highest values reported recently for microscale ZIF-8 (BET surface area = 1630 m^2/g, micropore volume = 0.64 cm^3/g) [31]. This finding possibly indicated that the as-synthesized nanoscale ZIF-8 contained residual species (e.g., unreacted Hmim) that cannot be desorbed from nanocrystal cavities in an activation step before the sorption measurements were performed [23].

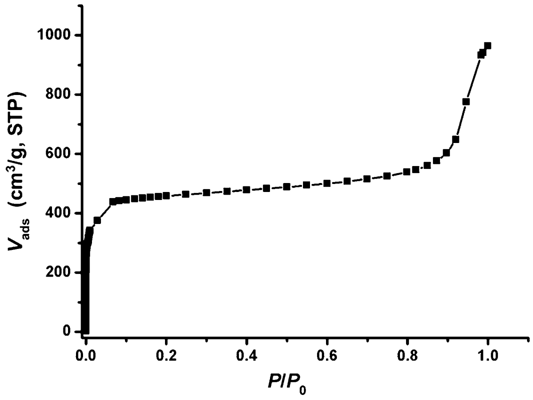

Fig. 2 Nitrogen physisorption isotherms (77 K) with a linear relationship

3.2 GCMC simulations for Kr and Rn adsorption

GCMC simulations were performed to determine the theoretical and practical possibilities of Rn adsorption on ZIF-8. Our GCMC simulation results are shown in Fig. 3.

The amount of adsorbed Rn on ZIF-8 did not increase as pressure increased. This result indicated that Rn adsorption by ZIF-8 was independent on pressure. Kr adsorption slightly differed from Rn adsorption.

Figure 4 shows the simulation results of Kr and Rn adsorption. Figure 4a, b reveal orthographic and van der Waals (vdW) radius views of Kr and Rn on ZIF-8. Although the vdW radius of Rn is slightly larger than that of Kr, the amount of adsorbed Rn is much higher than that of Kr because Rn exhibits stronger vdW interactions than Kr. Based on the fitting results of the parameters affecting Kr and Rn vdW interactions, the well depth of Rn (0.623 kcal/mol) is almost doubled compared with that of Kr (0.323 kcal/mol). Therefore, the strong interaction between Rn and ZIF-8 accounts for a high amount of adsorbed Rn.

Figure 4c, d shows the radial distribution functions (RDFs) of Kr and Rn to ZIF-8 atoms. The main difference

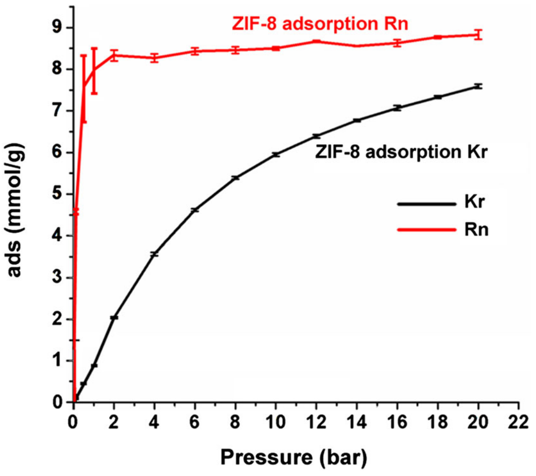

Fig. 3 (Color online) GCMC simulations of Rn and Kr adsorption by ZIF-8. *Red* and *black curves* correspond to Rn and Kr data, respectively

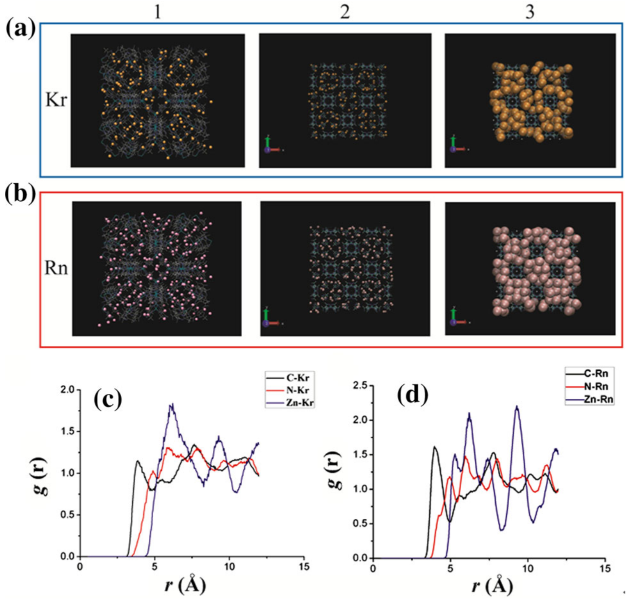

Fig. 4 (Color online) GCMC simulations of Rn and Kr adsorption. **a**, **b** Adsorption sites of Rn and Kr, respectively. **c**, **d** Radial distribution functions of adsorbed Rn and Kr, respectively

between the RDFs of Kr and Rn is that Rn atoms interact with ZIF-8 in a more orderly manner than Kr atoms. The corresponding peaks in both systems are found in similar locations. For example, the first carbon adsorbent peaks occur at approximately 4 Å, with that of Rn larger than that of Kr by <0.2 Å. Small peak location differences likely result from a larger adsorption amount and the corresponding tight packing of Rn because the vdW sigma value of Rn (4.10 Å) is larger than that of Kr (3.64 Å). This finding is confirmed by peak shapes. The RDFs of Rn are much more regular than those of Kr. The curvature of the RDFs of Rn represent ordered local structures even at atomic distances of >10 Å, particularly for the Zn–Rn pair. In C and N atoms, the RDF fluctuations of Rn are greater than those of Kr. Nevertheless, the shapes of these atoms are similar. The most distinct difference was observed between Zn–Kr and Zn–Rn pairs. Two small peaks split from the first major peak of the Zn–Rn RDF. These features indicated that the adsorbed Rn accumulated in crystal-like local structures.

3.3 Passive radon adsorption of ZIF-8

Rn and its decay isotopes contain a mixture of α, β, and γ rays. These α, β, and γ particles generated during Rn decay can be captured by a detector. The measurement results of radon adsorption on ZIF-8 (Fig. 5) are based on this principle.

Figure 5 shows that the amount of adsorbed Rn increased as adsorption time in the initial stage was extended (0–30 h). By contrast, The amount of adsorbed Rn between 30 and 36 h almost remained unchanged. Therefore, ZIF-8 is possibly saturated with adsorbed Rn between 30 and 36 h.

3.4 Active Rn adsorption by ZIF-8

3.4.1 Initial adsorption by α and β ray energy spectrometer measurements

The initial adsorption of Rn on ZIF-8 is investigated under different conditions. A fresh ZIF-8 material is used to adsorb Rn in α and β ray energy spectrometer measurements. The results show that 200 mg of ZIF-8 adsorbs approximately 1.06494 Bq of Rn (Fig. 6). This ZIF-8 material can be reused after a particular storage time. An equal weight of recycled ZIF-8 can also adsorb approximately 1.05517 Bq of Rn. These results demonstrated that ZIF-8 not only adsorbs radon but also maintains an adsorptive ability after recycling.

3.4.2 Initial adsorption by γ ray energy spectrometer measurement

The initial adsorption behavior of ZIF-8 was further investigated by monitoring γ ray energy emitted from adsorbed Rn. The results are summarized in Fig. 7. In fresh ZIF-8, 1 g of adsorbent cloud adsorbs approximately 8.653 Bq of Rn. The reused ZIF-8 adsorbent showed a similar adsorption capacity of 8.360 Bq.

The results demonstrated that ZIF-8 can be used and reused to adsorb Rn. Measurement results, except Rn concentration in a chamber, slightly differed because of the detection efficiencies of the two instruments. Experimental conditions were kept constant because environmental factors, such as relative humidity [32], likely affect Rn measurement.

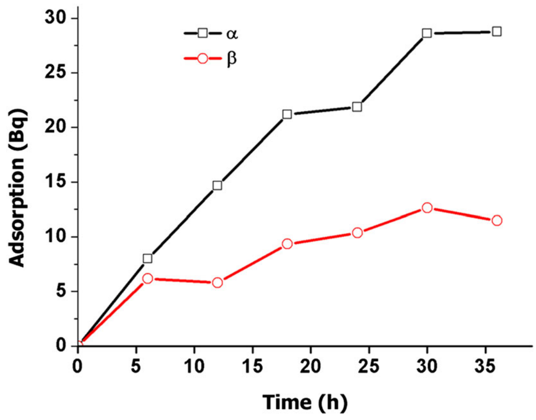

Fig. 5 (Color online) Passive Rn adsorption on ZIF-8

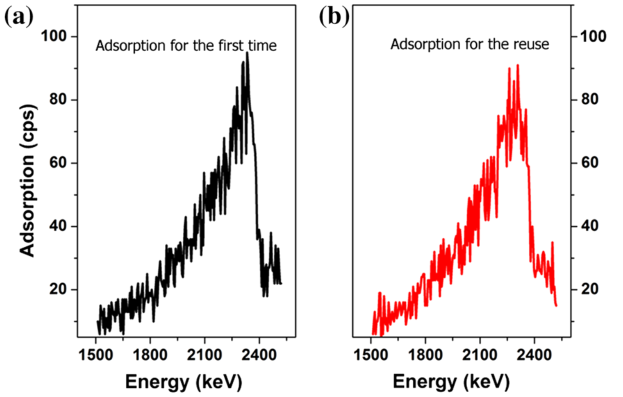

Fig. 6 (Color online) **a** ZIF-8 adsorption of radon for the first time. **b** ZIF-8 adsorption of radon for the second time

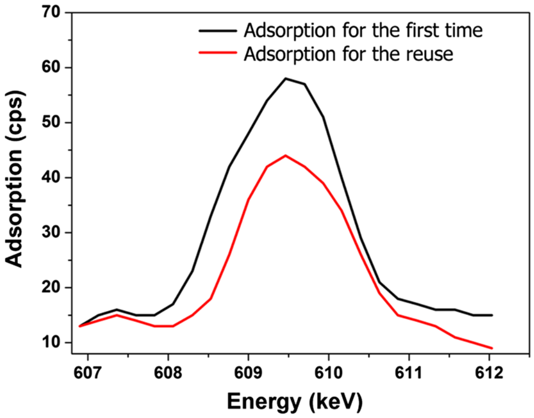

Fig. 7 (Color online) ZIF-8 adsorption of Rn

The mechanism by which Rn is adsorbed on ZIF-8 remains unclear. Under normal conditions, Rn is an inert gas; hence, this substance unlikely interacts with adsorbents. Therefore, adsorption may be dominated by vdW interactions between ZIF-8 and Rn. With this characteristic, Rn adsorbed on ZIF-8 becomes soluble in water and in organic media, such as fat. At 37 °C, the radon distribution ratio of fat to water is 125:1 [2].

Adsorbed Rn can be adsorbed whether ZIF-8, an example of a MOF, is reused or not. After ZIF-8 was used twice consecutively to adsorb Rn, the altered structures are almost similar to the original structures identified by XRD. This result demonstrated that ZIF-8 could not be disrupted after Rn was adsorbed once or twice (Fig. 8). Thus, the utilization efficiency of ZIF-8 can be improved. However, radon adsorption on ZIF-8 after several reuse cycles was not monitored.

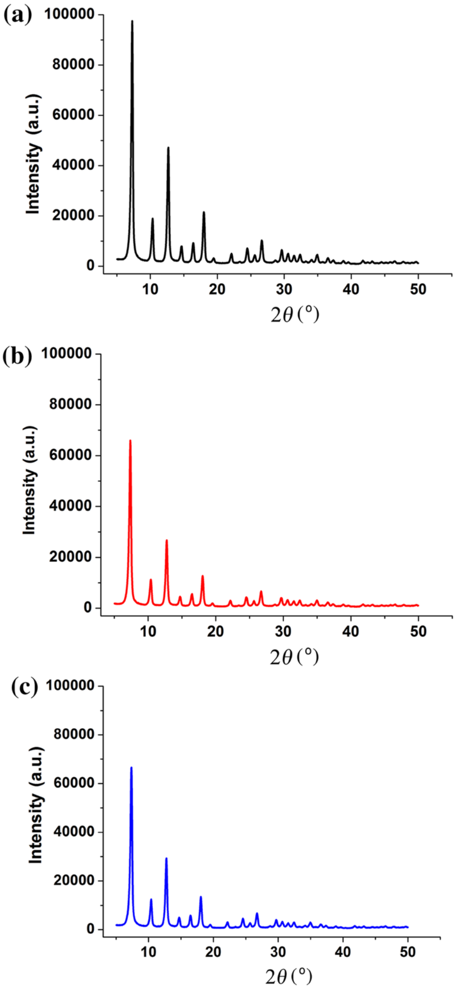

Fig. 8 (Color online) XRD spectra of ZIF-8 materials

4 Conclusion

This work demonstrated the adsorption behavior of radioactive Rn on ZIF-8. Theoretical simulations and experiments confirmed that ZIF-8 can be used to adsorb radioactive Rn. Considering that ZIF-8 is one of many existing MOFs, we believe that other MOFs may likely adsorb Rn. However, this assumption must be confirmed by further experiments to explore MOFs with enhanced surface area and appropriate pore structure to adsorb other isotopes of radioactive Rn.

Acknowledgments Supported by the Priority Academic Program Development of Jiangsu Higher Education Institutions (PAPD) and the Open Project of Jiangsu Provincial Key Laboratory of Radiation Medicine and Protection (No. KJS1246).

References

1. M. Khajeh, S. Laurent, K. Dastafkan, Nanoadsorbents classification, preparation, and applications (with emphasis on aqueous media). Chem. Rev. **113**, 7728–7768 (2013). doi:10.1021/cr400086v
2. S.P. Zhu, Z. Li, *Radiotoxicology*, 3rd edn. (Atomic Energy Press, Beijing, 1992), 289–291. (**in Chinese**)
3. S.D. Luo, Y.Q. Deng, F.Z. Dong et al., Evaluation method of radon preventing effect in underground construction. Nucl. Technol. **37**, 060501 (2014). doi:10.11889/j.0253-3219.2014.hjs.37.060501. (**in Chinese**)
4. M.M. Khin, A.S. Nair, V.J. Babu et al., A review on nanomaterials for environmental remediation. Energy Environ. Sci. **5**, 8075–8109 (2012). doi:10.1039/C2EE21818F
5. B.L. Chen, S.C. Xiang, G.D. Qian, Metal–organic frameworks with functional pores for recognition of small molecule. Acc. Chem. Res. **43**, 1115–1124 (2010). doi:10.1021/ar100023
6. J.R. Li, J. Sculley, H.C. Zhou, Metal–organic frameworks for separations. Chem. Rev. **112**, 869–932 (2011). doi:10.1021/cr200190s
7. B. Wang, A.P. Cote, H. Furukawa et al., Colossal cages in zeolitic imidazolate frameworks as selective carbon dioxide reservoirs. Nature **453**, 207–212 (2008). doi:10.1038/nature069007
8. O.V. Magdysyuk, F. Adams, H.-P. Liermann et al., Understanding the adsorption mechanism of noble gases Kr and Xe in CPO-27-Ni, CPO-27-Mg, and ZIF-8. Phys. Chem. Chem. Phys. **16**, 23908–23914 (2014). doi:10.1039/C4CP03298E
9. A.S. Dorcheh, D. Denysenko, D. Volkmer et al., Noble gases and microporous frameworks; from interaction to application. Microporous Mesoporous Mater. **162**, 64–68 (2012). doi:10.1016/j.micromeso.2012.06.004
10. M.V. Parkes, H. Demir, S.L. Teich-McGoldrick et al., Molecular dynamics simulation of framework flexibility effects on noble gas diffusion in HKUST-1 and ZIF-8. Microporous Mesoporous Mater. **194**, 190–199 (2014). doi:10.1016/j.micromeso.2014.03.027
11. Q. Wang, H. Wang, S. Peng et al., Adsorption and separation of Xe in metal–organic frameworks and covalent–organic materials. J. Phys. Chem. C **118**, 10221–10229 (2014). doi:10.1021/jp503255g
12. D.F. Sava, M.A. Rodriguez, K.W. Chapman et al., Capture of volatile iodine, a gaseous fission product, by zeolitic imidazolate framework-8. J. Am. Chem. Soc. **133**, 12398–12401 (2011). doi:10.1021/ja204757x
13. Y. Gurdal, S. Keskin, Predicting noble gas separation performance of metal organic frameworks using theoretical correlations. J. Phys. Chem. C **117**, 5229–5241 (2013). doi:10.1021/jp312838v
14. Z. Hulvey, K.Z.V. Lawler, Z. Qiao et al., Noble gas adsorption in copper trimesate, HKUST-1: an experimental and computational study. J. Phys. Chem. C **117**, 20116–20126 (2013). doi:10.1021/jp408034u
15. S.T. Meek, S.L. Teich-McGoldrick, J.J. Perry et al., Effects of polarizability on the adsorption of noble gases at low pressures in monohalogenated isoreticular metal–organic frameworks. J. Phys. Chem. C **116**, 19765–19772 (2012). doi:10.1021/jp303274m
16. C.A. Fernandez, J. Liu, P.K. Thallapally et al., Switching Kr/Xe selectivity with temperature in a metal–organic framework. J. Am. Chem. Soc. **134**, 9046–9049 (2012). doi:10.1021/ja302071t
17. J. Liu, P.K. Thallapally, D. Strachan, Metal–organic frameworks for removal of Xe and Kr from nuclear fuel reprocessing plants. Langmuir **28**, 11584–11589 (2012). doi:10.1021/la301870n
18. I. Halasz, P.J. Beldon, A. Belenguer et al., Real-time and in situ monitoring of mechanochemical milling reactions. Nat. Chem. **5**, 66–73 (2013). doi:10.1038/nchem.1505
19. S. Tanaka, K. Kida, M. Okita et al., Size-controlled synthesis of zeolitic imidazolate framework-8 (ZIF-8) crystals in an aqueous system at room temperature. Chem. Lett. **41**, 1337–1339 (2012). doi:10.1246/cl.2012.1337
20. Y.C. Pan, Y.Y. Liu, G.F. Zeng et al., Rapid synthesis of zeolitic imidazolate framework-8 (ZIF-8) nanocrystals in an aqueous system. Chem. Commun. **47**, 2071–2073 (2011). doi:10.1039/C0CC05002D
21. S. Tanaka, K. Kida, T. Nagaoka et al., Mechanochemical dry conversion of zinc oxide to zeolitic imidazolate framework. Chem. Commun. **49**, 7884–7886 (2013). doi:10.1039/C3CC43028F
22. K. Kida, M. Okita, K. Fujita et al., Formation of high crystalline ZIF-8 in an aqueous solution. Cryst. Eng. Comm. **15**, 1794–1801 (2013). doi:10.1039/C2CE26847G
23. J. Cravillon, S. Munzer, S.J. Lohmeier et al., Rapid room-temperature synthesis and characterization of nanocrystals of a prototypical zeolitic imidazolate framework. Chem. Mater. **21**, 1410–1412 (2009). doi:10.1021/cm900166h
24. A.K. Rappe, C.J. Casewit, K.S. Colwell et al., UFF, a full periodic table force field for molecular mechanics and molecular dynamics simulations. J. Am. Chem. SOC **114**, 10024–10039 (1992). doi:10.1021/ja00051a040
25. M.V. Parkes, C.L. Staiger, J.J. Perry IV et al., Screening metal–organic frameworks for selective noble gas adsorption in air: effect of pore size and framework topology. Phys. Chem. Chem. Phys. **15**, 9093–9106 (2013). doi:10.1039/c3cp50774b
26. H. Sun, COMPASS: an ab initio force-field optimized for condensed-phase applications-overview with details on alkane and benzene compounds. J. Phys. Chem. B **38**, 7338–7364 (1998). doi:10.1021/jp980939v
27. S.A. Moggach, T.D. Bennett, A.K. Cheetham, The effect of pressure on ZIF-8: increasing pore size with pressure and the formation of a high-pressure phase at 1.47 Gpa. Angew. Chem. Int. Ed. **48**, 7087–7089 (2009). doi:10.1002/anie.200902643
28. M.G. Martin, MCCCS Towhee: a tool for Monte Carlo molecular simulation. Mol. Simul. **39**, 1212–1222 (2013). doi:10.1080/08927022.2013.828208
29. K.S. Park, Z. Ni, J.Y. Choi et al., Exceptional chemical and thermal stability of zeolitic imidazolate frameworks. Proc. Natl. Acad. Sci. **103**, 10186–10191 (2006). doi:10.1073/pnas.0602439103
30. J.K. Zhao, L.Q. Ge, G.J. Zou et al., Experimental study on horizontal distribution of Rn concentration in confined chamber. Nucl. Technol. **36**, 110404 (2013). doi:10.11889/j.0253-3219.2013.hjs.36.110404. (**in Chinese**)
31. D. Van Der Spoel, E. Lindahl, B. Hess et al., GROMACS: fast, flexible, and free. J. Comput. Chem. **26**, 1701–1718 (2005). doi:10.1002/jcc.20291
32. W.C. Ding, J.H. Ruan, Q. Huang et al., Radon measurement in α energy spectrum and its influence factors. Nucl. Technol. **35**, 945–948 (2012). (**in Chinese**)